Journal of The Electrochemical Society, **166** (4) A605-A615 (2019)
0013-4651/2019/166(4)/A605/11/$38.00 © The Electrochemical Society

Application of Artificial Intelligence to State-of-Charge and State-of-Health Estimation of Calendar-Aged Lithium-Ion Pouch Cells

Ali Ghorbani Kashkooli, Hamed Fathiannasab, Zhiyu Mao, and Zhongwei Chen[z]

Department of Chemical Engineering, Waterloo Institute for Nanotechnology, Waterloo Institute for Sustainable Energy, University of Waterloo, Waterloo ON N2L 3G1, Canada

Accurate State-of-Charge (SOC) and State-of-Health (SOH) estimation of lithium-ion batteries (LIBs) is essential for the battery management system (BMS). For the first time, a feed-forward artificial neural network (ANN) has been used to estimate SOC of calendar-aged lithium-ion pouch cells. Calendar life data has been generated by applying galvanostatic charge/discharge cycle loads at different storage temperature (35°C and 60°C) and conditions (fully-discharged and fully-charged). The data has been obtained at various C-rates for duration of 10 months at one-month intervals. In order to include LIB hysteresis effect, two separate ANNs have been trained for charge and discharge data. The ANN have achieved a Root Mean Square Error (RMSE) of 1.17% over discharge data and 1.81% over charge data, confirming the ability of the network to capture input-output dependency. The calendar-aged battery data at various degradation conditions has been employed to train a new ANN to estimate SOH. The ANN has shown RMSE of 1.67%, demonstrating the network capability to estimate SOH. This study highlights the importance of considering aging effects in SOC estimates and the ability of ANN to include these effects efficiently.
 [DOI: 10.1149/2.0411904jes]

Manuscript submitted October 26, 2018; revised manuscript received February 4, 2019. Published February 23, 2019.

Lithium-ion batteries (LIBs) are the main choice of power source for portable electronics, grid energy storage systems, and electric vehicles (EVs).[1–3] However, recent trends in large scale electrification of vehicles has increased their demand significantly. Despite high energy and power density, capacity and power fade is a major concern for further expansion of EVs because of long calendar life requirement (up to 15 years).[4] The LIBs capacity and power fade can be ascribed to cycle aging and calendar aging. Calendar aging is especially important for EVs since the operation intervals is significantly shorter than the idle periods.[5] It is permanently present and includes all aging processes that lead to battery degradation independent of cycling[5] such as high ambient temperature or high state-of-charge (SOC) storage condition.[6] Whereas mechanical stress in electrode active materials and additives[7–9] or lithium plating[10–12] are responsible for cycle aging, the primary mechanism contributing to calendar aging is the evolution of a passivation layer at the electrode/electrolyte interface.[13,14] The formation and growth of passivation layer consumes the cyclable lithium in the system due to electrolyte decomposition. In addition, the growth of solid electrolyte interphase (SEI) at the anode is deemed to catalyze transition-metal ions dissolution from cathode, which are reduced at the anode surface.[15,16] The passivation layer growths and transitional-metal dissolution are enhanced by high temperature and the SOC in which they are calendared.[17,18] Therefore, a model that considers calendar aging should include the effects of temperature and SOC storage conditions.

SOC is defined as the ratio of battery remaining capacity to its nominal capacity. SOC estimation is a fundamental challenge in battery applications; Since the battery is an electrochemical storage system, the amount of its remained energy cannot be directly measured. SOC estimation is necessary for the reliable operation of EVs because it directly determines the remaining driving range.[19–21] SOC estimation is very challenging since it is highly non-linear function of ambient temperature and applied current.[22] On the other hand, LIB aging affects the electrodes structure, electrolyte composition, and their physio-chemical properties. Therefore, accurate estimation of SOC needs to consider the influence of cycle and calendar aging. There are numerous SOC estimation methods, Xiong et al. has classified them in 4 groups: 1) looking-up table based, 2) Ampere-hour integral, 3) model-based estimation, 4) data-driven estimation methods.[23] The first two was traditionally used and known to have their own limitations (for further details, see Ref. 23). Model-based estimates are very complicated and challenging to implement due to uncertainty in parameters of most models.[24] Model-based estimates use a battery model, expressed as a state equation, then, a nonlinear state estimation algorithm along with an adaptive filter is employed to deduce the battery SOC. Model-based methods are designed to automatically self-adjust themselves with the system dynamics.[25] Common algorithms include Luenberger observer,[26,27] PI (proportion integration) observer,[28] sliding mode observer,[29] and Kalman filter (KF).[30] KFs and its derivatives are the most accepted methods and are extensively used.[31–33] Top battery monitoring patent holders consist of EV makers and battery manufacturers having various SOC estimates methodologies. For example, in case of ampere-hour integral SOCs, General Motors developed an ampere-hour integral and open circuit voltage-based method called startup SOC and running SOC;[34,35] Tesla proposed a weighting function applied on the old capacity values to update the current capacity and SOC.[36] In case of model based SOCs, General Motors developed a dynamically adaptive method using first-order equivalent circuit model;[37] Ford proposed a nonlinear observer along with a first-order equivalent circuit model;[38] LG Chem proposed an adaptive method using dual extended Kalman filtering to determine the time-varying parameters of an electrochemical cell model for the SOC estimation.[39] The LG Chem electrochemical battery model improved the accuracy of SOC estimate, however, it made the SOC estimate more complex compare to the first-order equivalent circuit models.

With recent development of artificial intelligence and deep learning,[40] data-intensive scientific discovery has gained a lot of attention.[41] Data-driven methods only use battery state variable measurements as the input and SOC as the output to map a model between inputs-output. LG Chem proposed data-driven methods using an ANN having cell's temperature, voltages, currents and time as the input and SOC as the output.[42,43] They recommended employing these methods where the high precision of SOC estimation is required such as hybrid EVs. Data-driven methods have higher prediction accuracy compared to traditional models due to the absence of modeling simplifying assumptions. They involve data science and rely on advanced machine-learning (ML) algorithms to determine SOC. This provide other potential advantages of data science including parallel distribute processing, high computation rates, fault tolerance, and adaptive capability.[23] ML allows computers to learn pattern in data without previous knowledge between input and output. In the near future, it deems to transform most industries to be smarter and will be deeply involved in our daily lives. There are countless ML techniques available, however, the main associated with SOC estimation includes artificial neural network (ANN),[29,30] fuzzy logic-based,[46,47] and support vector machine (SVM).[48,49] Since KFs have proven to be successful for SOC estimation, they have also been implemented together with ML methods.

[z]E-mail: zhwchen@uwaterloo.ca

The literature showed that such hybrid methods could produce more accurate results compared to individual methods.[24] Using ANN and extended KF, Charkhgard et al. estimated the SOC at room temperature with the root mean square error (RMSE) of 2%.[50] Moreover, Meng et al. combined unscented KF with SVM to predict the SOC with a mean absolute error (MAE) below 2%.[51] Recently, Chemli et al. used only one individual deep feedforward neural network to map battery drive cycle measurements to SOC without using any complementary model. They achieved MAE of 1.10% over a 25°C dataset and 2.17% over at −20°C dataset.[45] All SOC estimation studies in literature have neglected battery calendar aging. However, for the accurate SOC estimation, the battery calendar aging and its effect on the cell capacity needs to be considered.

In addition to SOC, state-of-health (SOH) of the battery also needs to be monitored by BMS.[52] The SOH demonstrates a battery energy storage and delivery capability compared to its original condition. When the battery is fresh, SOH equals to 100% and decreases as the battery ages. SOH is determined by the application requirements. SOH determines the end of life of a battery, e.g. when it reaches the 80%, the battery is no longer suitable for EV application and needs to be replaced.[53] SOH estimate is typically expressed as the reduction of the battery capacity or the battery power.[54] Classical methods to estimate SOH were destructive and required cell destruction. However, model based and data-driven methods such as fuzzy logic,[29] KF,[55] and ANN[50] offer SOH by a non-destructive way. These methods commonly provide SOH and SOC together.

In this paper, SOC and SOH of calendar-aged lithium-ion pouch cells have been estimated using a data-driven method. The battery dataset is obtained from the calendar-life experiment of eight commercial 15 Ah LIB pouch cells. The effect of different storage temperatures and storage conditions (either fully-discharged or fully-charged) have been considered in calendar-life study. All cells have graphite as the anode and blended $LiNi_xMn_yCo_{1-x-y}O_2$-$LiMn_2O_4$ (NMC-LMO) as the cathode. The battery measurements are involved galvanostatic charge/discharge cycling at various C-rates and conducted at one-month interval for a period of 10 months. SOCs and SOHs are estimated based on a feed-forward ANN model via Matlab/ANN Fitting app. It is shown that the ANNs are able to estimate the SOC and SOH of calendar-aged pouch cells with high accuracy. This paper is organized as follows: first, the experimental method used to obtain the battery measurements is described. Then, the theoretical background to train the ANN are presented. Finally, the ANN results are presented and discussed with concluding remarks.

Experimental

The calendar-life experiment was performed on commercial lithium-ion pouch cells having a nominal capacity of 15 Ah. The cells were originally designed for plug-in hybrid EVs and have a NMC-LMO blended and graphite as positive and negative electrodes, respectively. The effects of charged/discharged storage conditions and temperature on the calendar-life was investigated. More experimental details can be found in our previous paper[56] and is briefly explained here.

Two cells were stored in each of the following four conditions: fully-discharged at 35°C, fully-discharged at 60°C, fully-charged SOC at 35°C, and fully-charged at 60°C (total of 8 cells). Having 2 batteries tested in each condition allowed the determination of variability in cell voltage and capacity at each condition. Each new, as-received, cell had initial 50% SOC. It was initially tested to confirm its capacity and rate capability, then was discharged to 0% or charged to 100% depending on the experiment requirement using a battery cycler (MACCOR model 4200, USA). In this study, the battery is assumed to be fully-charged (100% SOC) at 4.15 V and fully-discharged (~40% SOC) at 2.8 V. The capacity and rate capability of each cell was determined by employing constant-current-constant-voltage (CC-CV) charge/discharge cycling protocol; The CC-CV cycle comprises the following steps: 1) a galvanostatic discharge at a specified C-rate until a cutoff voltage of 2.8 V reached; 2) a discharge at constant voltage until the cell current dropped below C/20; 3) 10 minutes of rest; 4) cell charging at the same C-rate until to reach charging cutoff voltage of 4.15; 5) charging continued at constant voltage until the C/20 current was reached; 6) 10 minutes of rest. The cells charge/discharge cutoff voltages were selected based on the manufacturer recommendation. The cells rate capabilities were determined at C/5, C/2, 1C, and 2C. The C-rates are based on the nominal capacity of 15 Ah. The cells had 3 conditioning CC-CV cycles at 1C before the rate capability testing.

Two fully-discharged SOC cells and two fully-charged cells were placed in a temperature-controlled environment at 35°C, whereas two fully-discharged cells and two fully-charged cells were stored at 60°C. All cells were kept at open-circuit in temperature-controlled chambers. In order to detect degradation of the cells, their performance was measured at 1-month intervals for 10 consecutive months using the following procedure. The cells were removed from the chamber and then cooled to the room temperature and were allowed to rest for 4 hours before conducting 1C cycling and rate capability tests. After recording the cell rate capability test, the cells were restored back to their initially assigned storage conditions (fully-discharged or fully-charged). Afterward, the cells were moved back to the temperature-controlled chamber. Because the cell capacity degraded during aging experiment, the fully-discharged and fully-charged are set to be states in which the cell voltage reaches the cutoff voltage of 2.8 V and 4.15 V, respectively. Therefore, the battery is assumed to be fully charged (100% SOC) at 4.15 V and fully discharged (0% SOC) at 2.8 V. The cell maximum capacities at the end of C/5 CC-CV were recorded and used for SOH estimation.

Theoretical Background

SOC estimation.—The SOC is defined as the ratio of current capacity (Q(t)) to the nominal capacity or rated capacity (Q_n).[24] Q_n is the amount of energy that can be drawn from the battery when it is fully-charged and is provided by the manufacturer.[44] The constant current used to rate the battery varies from manufacturer to manufacturer and is typically either C/10, C/20, or C/100. SOC in EVs is similar to the "Gas Gauge" in internal-combustion-engine vehicles and is a measure of the short term battery capability. The SOC at each time during battery operating time is defined as:[44]

$$SOC\,(t) = \frac{Q\,(t)}{Q_n} \qquad [1]$$

In this study, to estimate SOC, ANN was chosen that mimics the functioning of human brain.[57,58] In a neural network, the artificial neuron receives one or more inputs and sums the weighted inputs to produce an output. There are many ANN methods available, among them, Multi-Layer-Perceptron (MLP) is chosen. MLP simulates the human brain behavior by forming complex network of interconnected nodes. The nodes spread over several layers including one input layer, one or more hidden layers, and one output layer. The MLP network is feed-forward, meaning that the connection between different layers is in one direction from the input to the output. Each layer, except input layer, processes the information from the previous layer and send the result to the next layer.[54] In this study, an MLP use the history of battery measurements during calendar-life experiment to map 5 inputs to the output. Inputs are cell voltage, current, aging time (month), storage temperature, and storage condition (fully-discharged or fully-charged) and the output is the current SOC.

The architecture of MLP used to determine aged-batteries SOC, is shown in Fig. 1. The MLP has an input layer, a hidden layer, and an output layer. MLP with one hidden layer can approximate any continuous function.[57] Input layer has 5 neurons, hidden layer has m neurons (will be determined later), and output layer has only one neuron. The nodes in each layer are related to nodes in the next layer with a weight w_{ij}. The total input of a hidden neuron i is computed using weights and bias of each layer as:[24]

$$net\ i_j = \sum_{i=1}^{n} w_{ij}x_i + b_j \qquad [2]$$

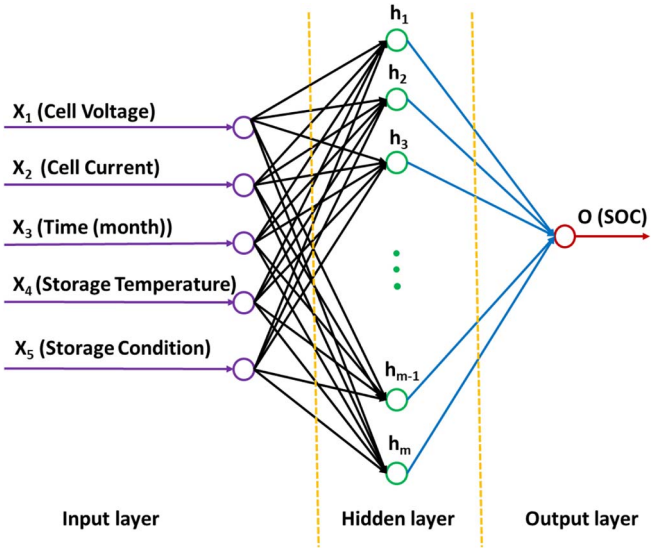

Figure 1. The MLP architecture for SOC estimation of calendar-aged batteries.

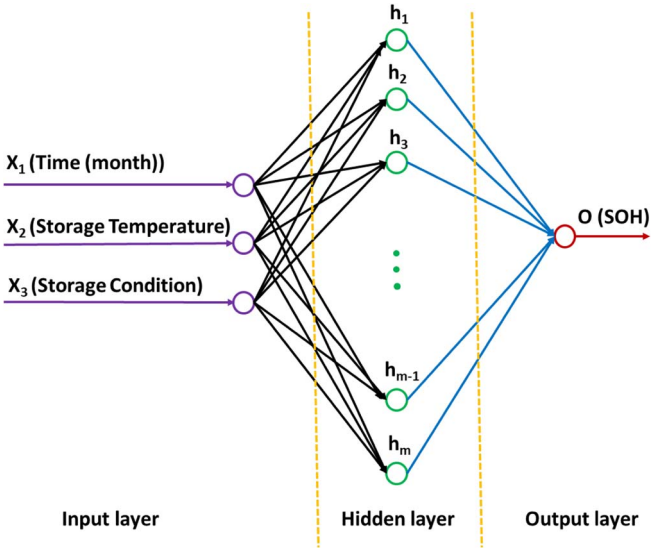

Figure 2. The MLP architecture for SOH estimation of calendar-aged batteries.

where i_j is total input of the hidden layer neuron j, x_i is input to the hidden layer neuron i and hidden layer neuron j, b_j is bias of the hidden layer neuron j (bias term is similar to intercept in linear regression). The activation function is applied on the total input and provides the output of the hidden neuron to the next layer as:

$$h_j = f\left(net\ i_j\right) = \frac{1}{1+\exp\left(-net\ i_j\right)} \quad [3]$$

It is possible to use different activation functions on hidden layer, e.g. hyperbolic tangent. However, we selected sigmoid function for this study.

The total input of the neuron o is computed using:

$$net\ o = \sum_{i=1}^{p} w_i h_i + k \quad [4]$$

where $net\ o$ is total input of output layer (neuron o), w_i is the weight associated with the hidden layer neuron i and output layer neuron, k is the bias of the neuron in output layer o; p is the number of neurons in the last hidden layer. The linear activation function is applied to $net\ o$ in output layer:

$$o = f(net\ o) = net\ o \quad [5]$$

SOH estimation.—A fresh fully charged battery has the maximum releasable capacity (Q_{max}). As the battery ages, Q_{max} declines due to the cycling and calendared aging. Therefore, it can be used to estimate the battery health using SOH defined by:

$$SOH = \frac{Q_{max}}{Q_n} \quad [6]$$

SOH estimation is important to quantify the degradation of the battery and prevent the failure of EVs before happening. In this study, the CC-CV capacity at the end of C/5 discharge is used as Q_{max} for SOH estimation. An MLP is used to model the SOH of the calendar-aged pouch cell. The MLP maps aging time (month), storage temperature, and storage condition (as inputs) to the SOH (as output). The architecture of SOH estimating using MLP is shown in Fig. 2. The ANN includes an input layer, a hidden layer, and an output layer. Input layer has 3 neurons, hidden layer has m neurons, and output layer has only one neuron of SOH. Similar to SOC network, the sigmoid and linear activation functions are used on hidden and output layers, respectively.

Model training.—When training an ANN, dataset is randomly divided into three separate training, cross-validation, and test sets. The model is formed using only the training dataset. During training, cross-validation dataset is used to evaluate the model's ability to predict new data that was not used in training. After training, test dataset is used to evaluate the trained network. 70 percent of measurement data is used for training, 15% for cross-validation, and 15% percent for testing. Data was divided randomly between 3 groups to minimize the effects of sampling bias.[41] Levenburg-Marquardt algorithm is used to train the ANN[59] and the Mean-Square-Error (MSE) was chosen as the metric to evaluate the performance of the MLP. MSE measures the average of square of errors between the predicted values and what is predicted and includes both the variance and bias of the predicted value. MSE is a measure of the quality of the model and is defined by:

$$MSE = \frac{\sum_{i=1}^{n}(y_i - \widehat{y_i})^2}{n} \quad [7]$$

In this equation, y_i is the experimentally measured value and $\widehat{y_i}$ denotes the predicted value, n represents the number of observations.

Results and Discussion

MLP maps the battery measured data to SOC. The data was recorded in 10 s intervals resulting in time series data (total of 249206 records) at various operating conditions. The dataset consists of voltage ranging from 2.8 V to 4.15 V, current (0.2C-0.5C-1C-2C), aging time (0 to 10 month), storage temperature (35°C–65°C), storage condition (fully-discharged-fully-charged), and capacity. The first five features are used as input and the last one is used as output. Fig. 3 shows a sample of battery discharge curves obtained after 8 months at various C-rates and aging conditions. Fig. 3 shows that rising storage temperature does not accelerate calendar aging when the battery stored at fully-discharged condition. However, when the battery is stored in fully-charged condition at elevated temperature, the capacity fade is significant after 8 months, (see Fig. 3d). More discussion about cells degradation can be found in our previous paper.[56]

Similar figures could be made for other months and total data includes for all months from 0 to 10 was used in the MLP architecture shown before, (see Fig. 1). The input values are normalized between 0 and 1 by dividing them by absolute maximum input values. The output (capacity) was normalized by nominal capacity that represents SOC. Storage temperature of 35°C and 65°C is mapped to 0 and 1, respectively. Similarly, fully-discharged and fully-charged storage conditions are represented by 0 and 1.

There are 1 input layer (5 neurons), 1 hidden layer (4 neurons) and 1 output layer (1 neuron) in the ANN architecture. There are 4

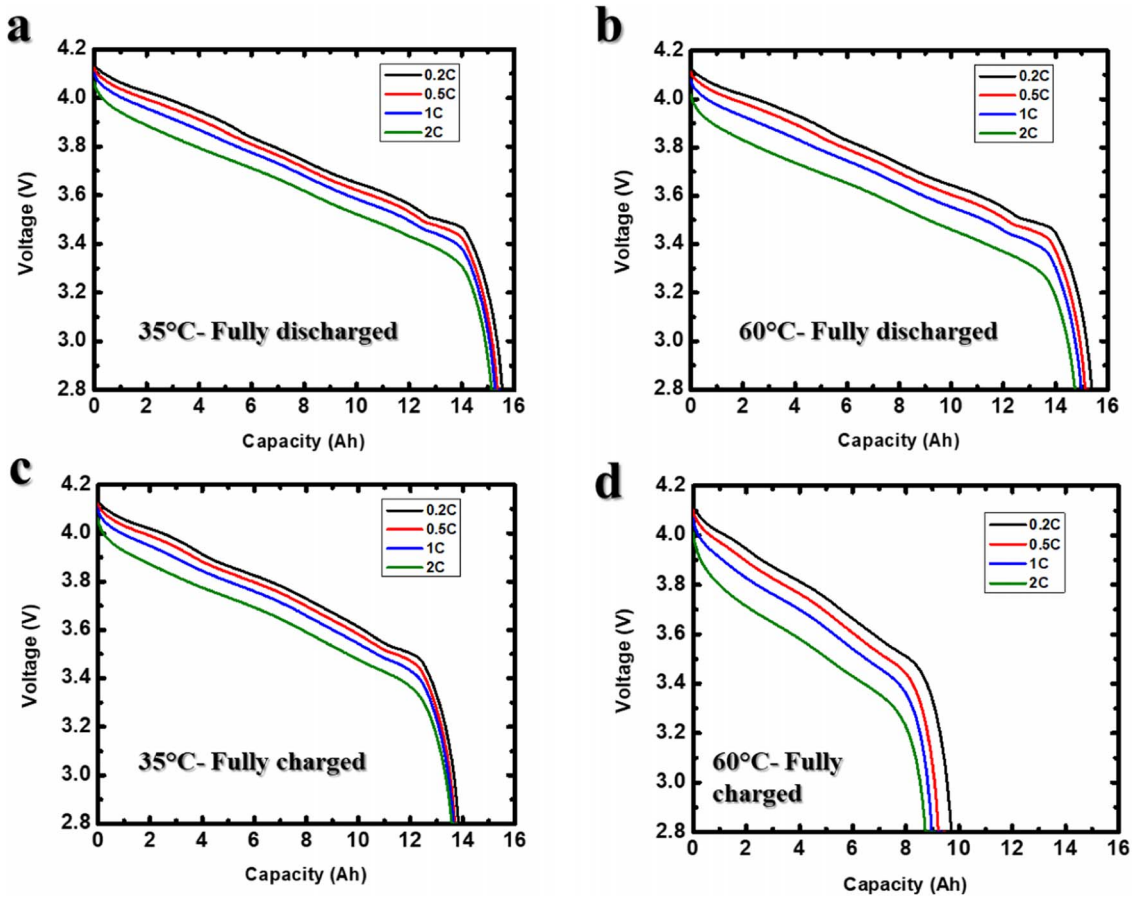

Figure 3. Galvanostatic discharge curves obtained at various current densities from aged-pouch cells after 8 months at various degradation conditions.

neurons in hidden layer determined by trial and error. The training process stops either the gradient falls below 10^{-7}, or MSE becomes 0, or validation checks become greater than 6. Fig. 4 shows the MSE as the function of epochs for train, validation, and test datasets. It takes 87 epochs to train the network where the maximum validation checks of 6 is met. The MSE of 1.38×10^{-4} is achieved over test dataset. This equals to RMSE of 1.17% which is below the 2% reported using ANN and extended KF.[50] The ANN training result is summarized in Table I along with MSEs for different training/validation/test datasets. The training and validation errors are in the same order of magnitude, confirming the model can generalize well.

The MSE variation for train, validation, and test datasets at different epochs is shown in Fig. 4a. green circle shows the best network performance. Fig. 4b represents the error histogram for different datasets.

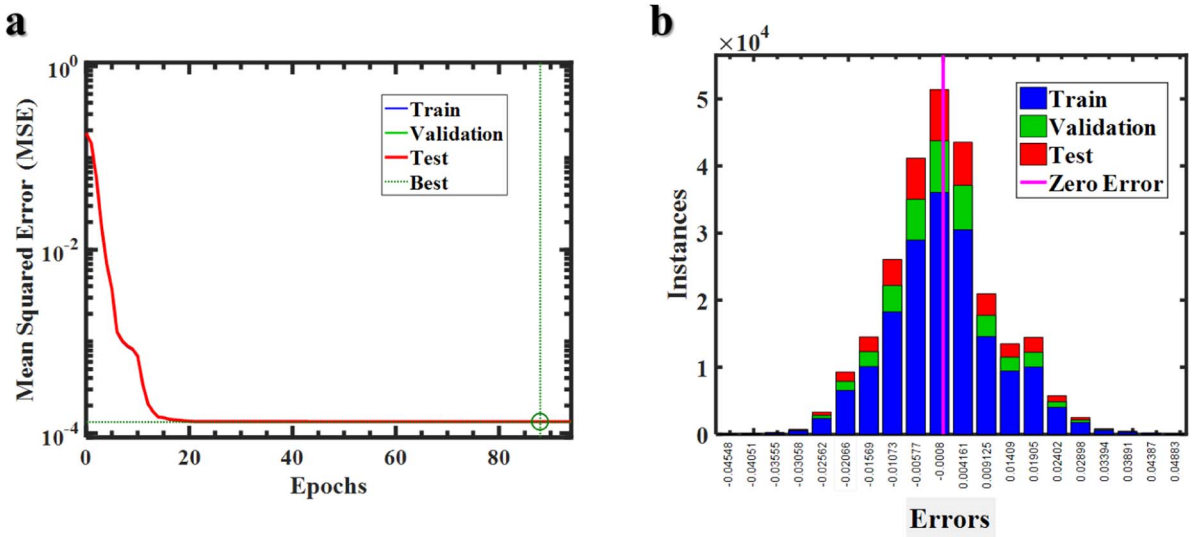

Figure 4. a) MSE for train, validation, and test datasets at different epochs for discharge data, b) Error histogram which is the difference between target and ANN output.

Table I. Training results of ANN based on discharge data.

Training Parameters	Value
Training Algorithm	Levenberg-Marquardt
Metric	Mean Squared Error
Epochs	87
Performance	1.38×10^{-4}
Training performance	1.39×10^{-4}
Validation performance	1.34×10^{-4}
Test performance	1.43×10^{-4}
Gradient	2.51×10^{-7}
μ	1×10^{-5}
Validation Checks	6

Errors are the difference between the targets and ANN outputs. Target is the SOCs obtained based on experiment. Fig. 4b demonstrates that errors are concentrated close to zero with the maximum range of 0.03. The errors of high performance ANN are distributed close to the zero. This confirms the ANN accuracy to capture the target.

Fig. 5 compares the SOC calculated from experiment during a discharge at various C-rates after 8 months of aging (stored at 60°C-Fully charged) with the one predicted by ANN. The results show that the ANN can successfully predict the battery SOC during galvanostatic discharge process at different C-rates. The choice of months = 8 is quite arbitrary and similar plots can be made for other months.

As mentioned, for the accurate SOC estimation, the calendar aging features including storage temperature and fully-charged/discharged storage conditions needs to be considered. In order to further elucidate this point, a new ANN is trained using the discharge dataset without considering the calendar aging features (temperature and fully-charged/discharged storage conditions). The MSE of ANN without aging features is almost 60 times higher than the one includes aging features (8.51×10^{-3} vs 1.38×10^{-4}), confirming the importance of including aging features in the SOC estimates. Fig. 6 compares the ANN prediction with aging and without aging features to the measured battery data. It demonstrates that ANN without aging features fails to predict the SOC of calendar-aged cells after 8 months of aging (stored at 60°C-fully charged) at various C-rates.

In order to show the ANN capability to predict unknown data, the data related to one month could be excluded from the training dataset. Next, the trained ANN will be used to predict the excluded dataset. For this, we excluded the months = 8 data from training set and used the newly trained ANN to predict the SOC for month = 8. Fig. 7 shows the predicted SOC excluding months = 8 data from the training and compare it with battery measured. The ANN can accurately predict the SOCs, confirming its capability to use the current data for training and predict unknown SOC in completely new condition.

Up to this point, we have only used discharge data to train ANN for SOC estimation. However, the SOC can be estimated based on charge data. The idea behind separating charge and discharge data is that there is an asymmetry in the discharge/charge profiles of LIBs. Mao et al. showed that there is an asymmetry in the performance of blended NMC-LMO cells during charge and discharge.[60] This hysteresis effect is a characteristic of LIBs in which changing the current direction from charge to discharge, the output voltage does not follow back

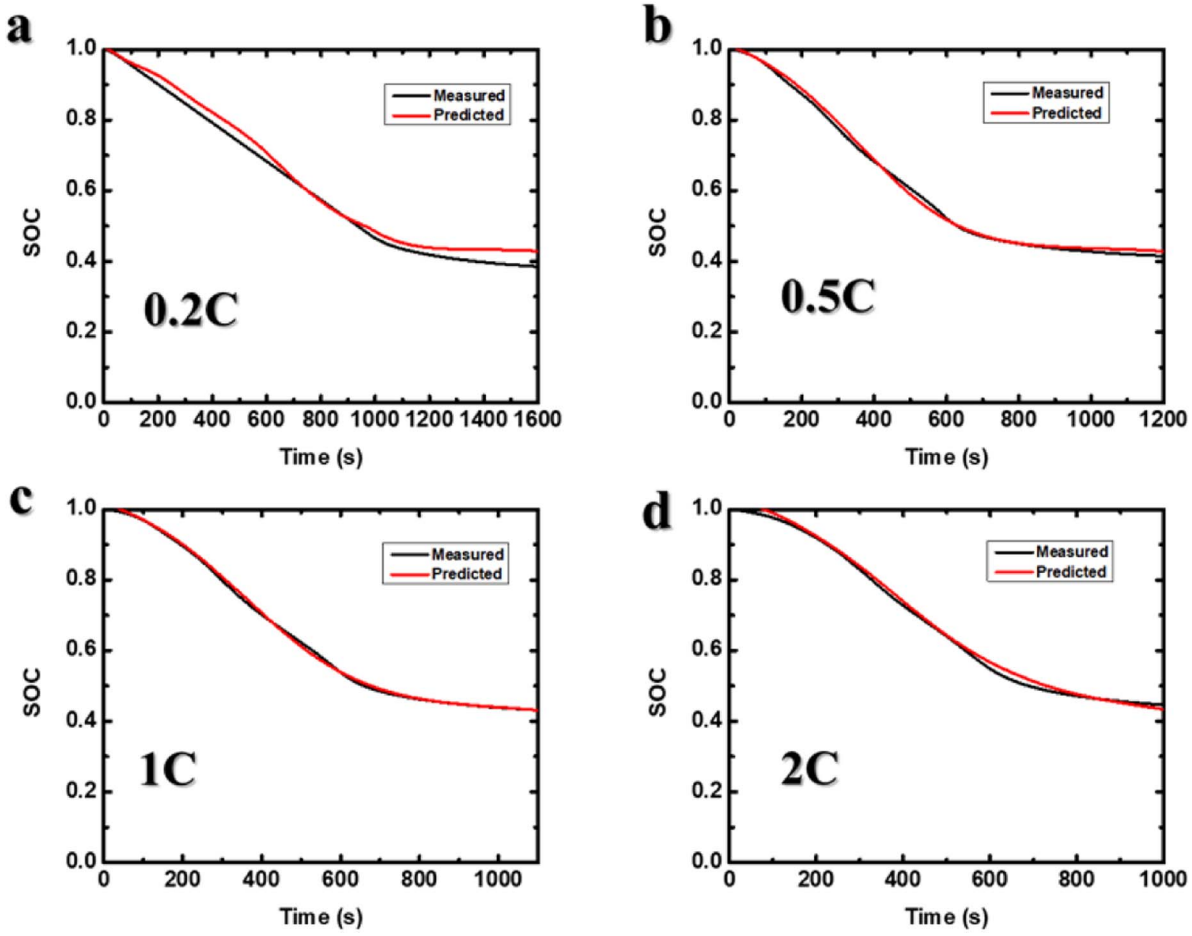

Figure 5. SOC after 8 months of aging (stored at 60°C-Fully charged) during discharge at various rates a) 0.2C b) 0.5C c) 1C d) 2C, measured (black) and ANN prediction (red).

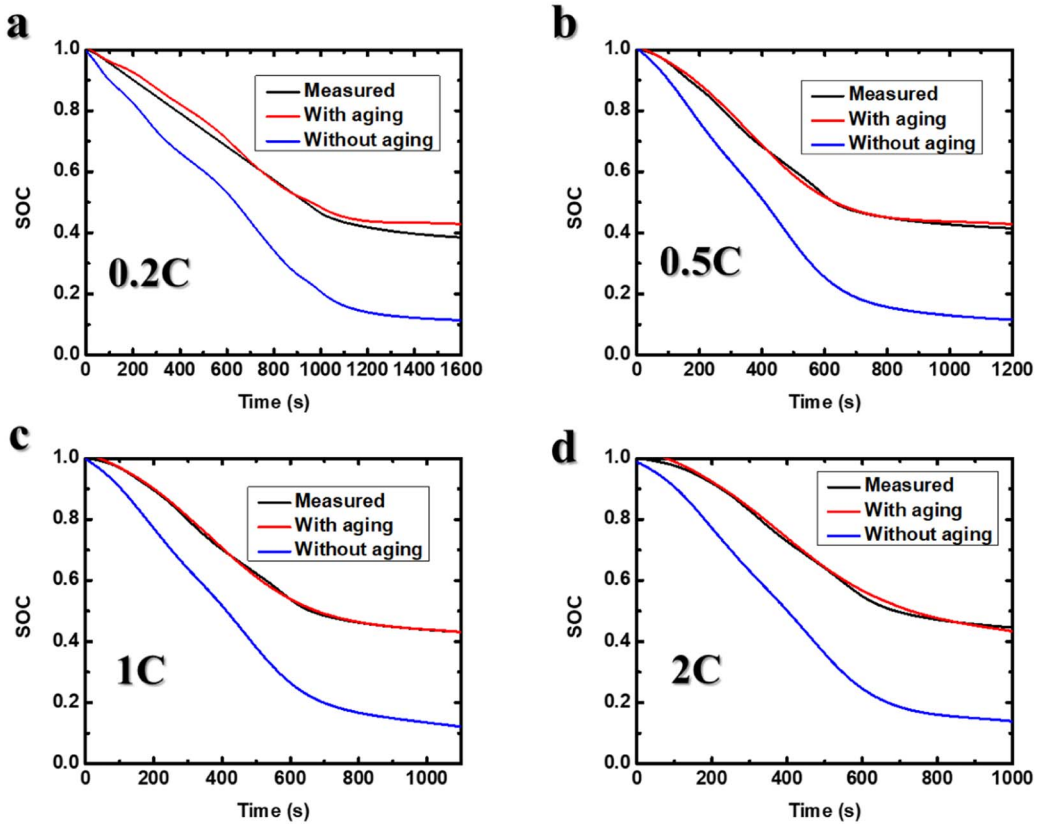

Figure 6. SOC after 8 months of calendar aging (stored at 60°C and fully-charged) during discharge at various rates a) 0.2C b) 0.5C c) 1C d) 2C, measured (black), includes aging features (red), without aging features (blue).

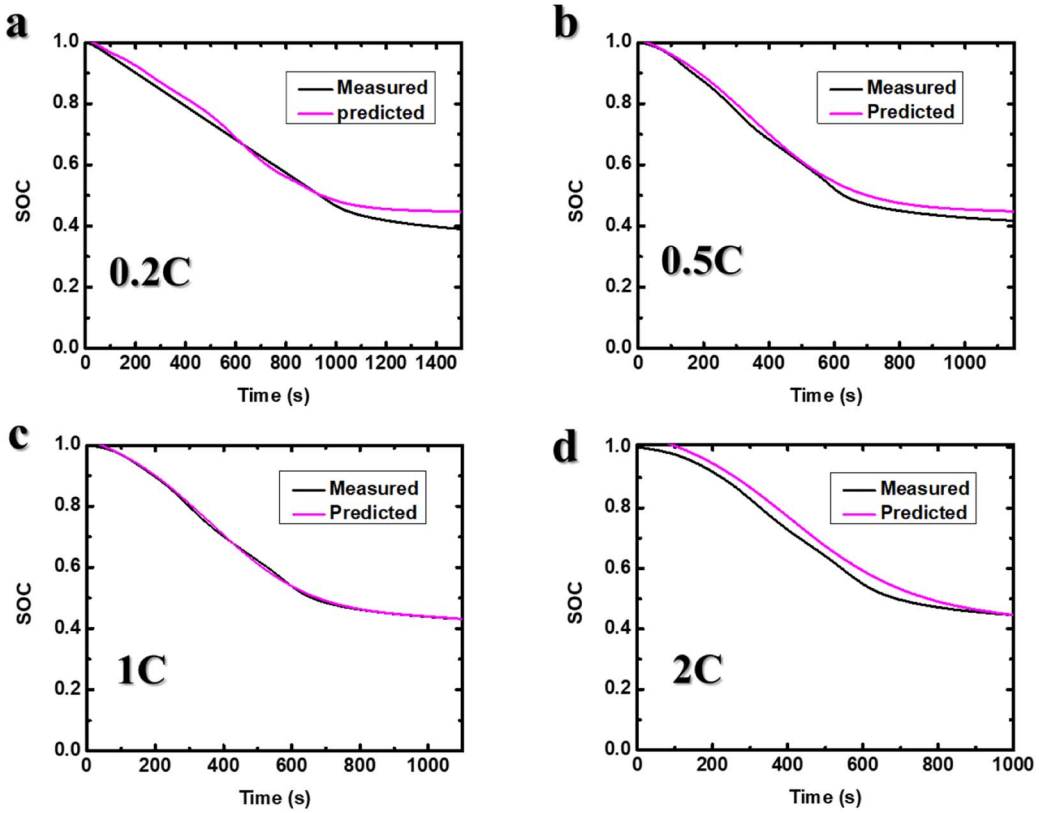

Figure 7. SOC after 8 months of aging (stored at 60°C- fully-charged) during discharge at various rates a) 0.2C b) 0.5C c) 1C d) 2C, measured (black), ANN prediction excluding month 8 data from training (pink).

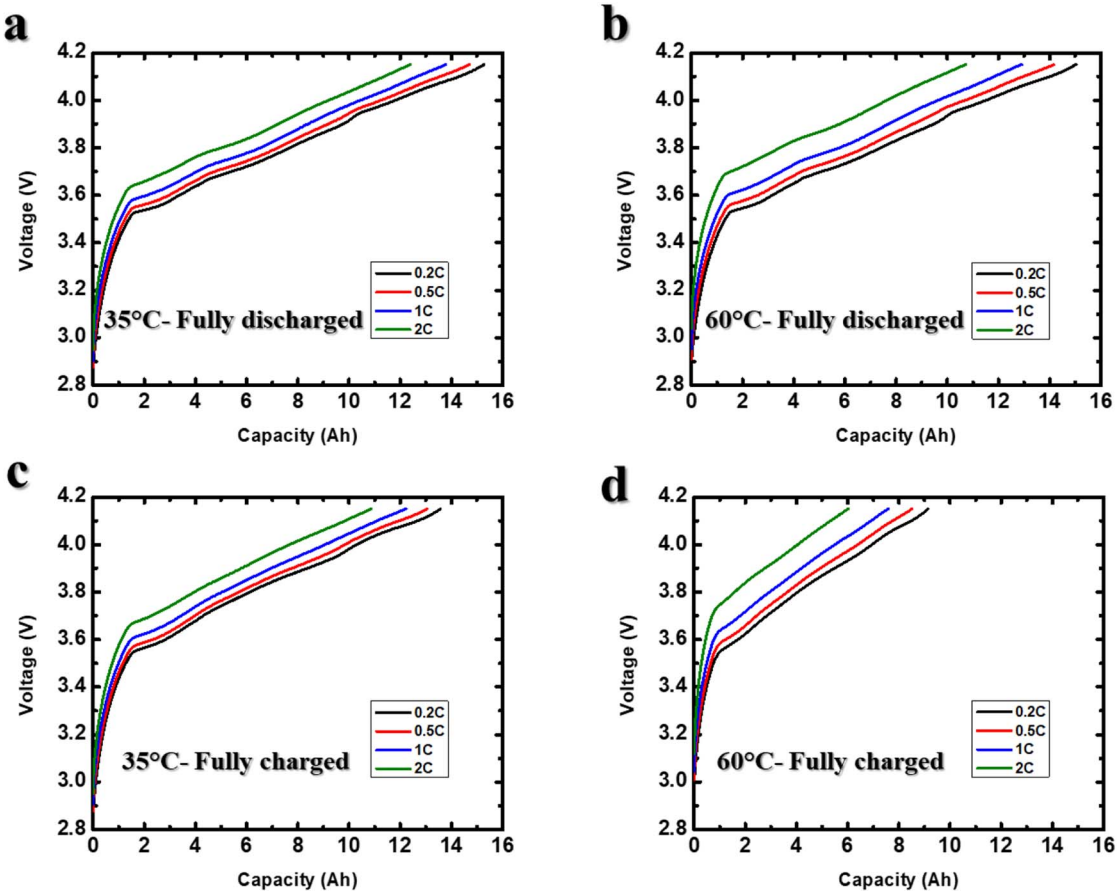

Figure 8. Galvanostatic charge curves obtained at various current densities from aged-pouch cells after 8 months at various degradation conditions.

the previous profile. It was shown that OCV after a previous charge is typically higher than the OCV after discharge at the same SOC value.[61] In order to include the charge/discharge asymmetry, the charging data was used to train a new ANN, with the similar architecture as shown in Fig. 1, for charging process. Fig. 8 shows the cell charging data after 8 months under the various aging conditions. Fig. 8 demonstrates that rising storage temperature does not influence capacity delivery of battery when it is stored fully-discharged. However, when it is stored fully-charged at elevated temperature, the charging capacity decreases significantly after 8 months, (see Fig. 3d).

The charge data (total of 232733 points) is used as the dataset to train a new ANN. There are 6 neurons in hidden layer determined by trial and error. It takes 102 iterations to train ANN where the maximum validation check is satisfied. The training results are given in Table II. The MSE of 3.29×10^{-4} is achieved over test dataset equals to RMSE of 1.81%. The MSE variation for train, validation, and test datasets is shown in Fig. 9a. Fig. 9b represents the error histogram for different datasets. Fig. 9b demonstrates that errors are focused close to zero with the maximum range of 0.01. This demonstrates that the ANN predicts the target data with high accuracy. Fig. 10 compares the SOC obtained from experiment after 8 months of aging (stored at 60°C-Fully charged) during charge at various C-rates with the one predicted by ANN. The results show that the ANN can successfully predict the SOC during galvanostatic charge process at different C-rates.

Similar ANN could be trained using the dataset obtained from the second batteries tested at the same condition of first batteries. Originally dataset 1 was used to present the previous results. Table III

Table II. Training results of ANN based on charge data.

Training Parameters	Value
Training Algorithm	Levenberg-Marquardt
Metric	Mean Squared Error
Epochs	102
Performance	3.29×10^{-4}
Training performance	3.37×10^{-4}
Validation performance	2.89×10^{-4}
Test performance	3.15×10^{-4}
Gradient	4.19×10^{-7}
μ	1×10^{-8}
Validation Checks	6

Table III. MSE of ANNs based on two datasets obtained from the testing at the same condition.

	Discharge data			Charge data		
	Training	Validation	Test	Training	Validation	Test
Dataset 1	1.39×10^{-4}	1.34×10^{-4}	1.43×10^{-4}	3.37×10^{-4}	2.89×10^{-4}	3.15×10^{-4}
Dataset 2	5.44×10^{-4}	5.59×10^{-4}	5.45×10^{-4}	2.46×10^{-4}	2.54×10^{-4}	2.47×10^{-4}

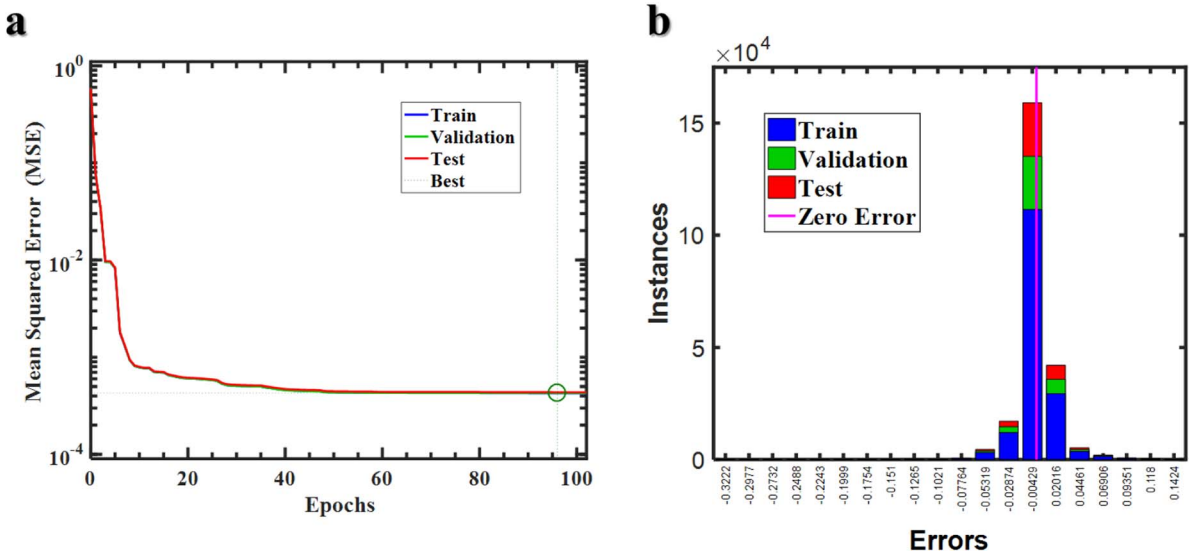

Figure 9. a) MSE for train, validation, and test datasets at different epochs for charge data, b) Error histogram which is the difference between target and ANN output.

compares the MSE calculated for training, cross-validation, and testing datasets for the two sets of batteries tested at the same conditions, showing similar MSEs between two datasets. Then, the ANN trained using dataset 1 is used to predict the measured SOC based on dataset 2, confirming the reliability of ANN model to generalize for similar batteries tested at the same condition (see Fig. 11).

Finally, an ANN shown in Fig. 2, is employed to estimate the SOH. CC-CV discharge capacities at the end of C/5 discharge are used as

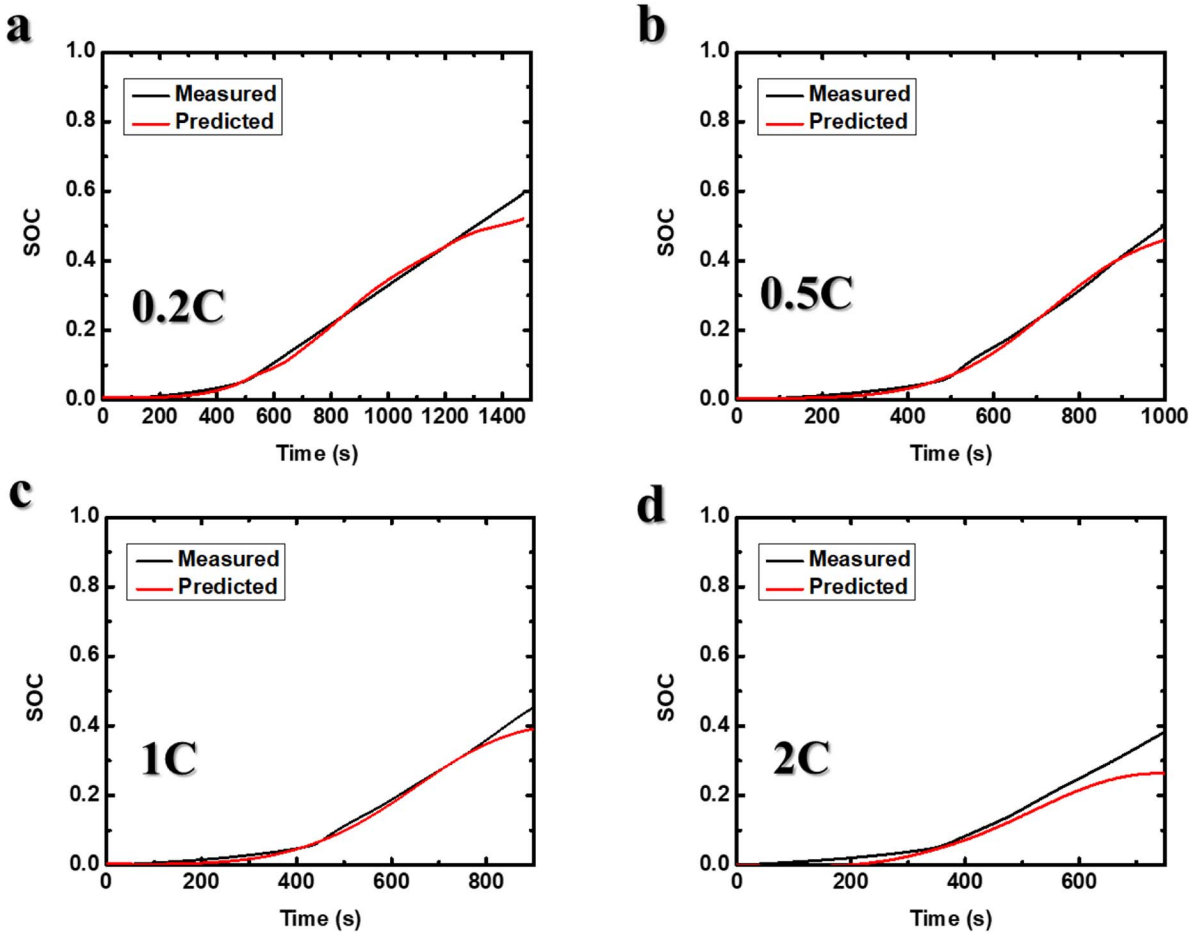

Figure 10. SOC after 8 months of aging (stored at 60°C-Fully charged) during charge at various rates a) 0.2C b) 0.5C c) 1C d) 2C, measured (black) and ANN prediction (red).

Table IV. Training results of ANN for SOH estimation.

Training Parameters	Value
Training Algorithm	Levenberg-Marquardt
Metric	Mean Squared Error
Epochs	20
Performance	2.85×10^{-4}
Training performance	2.70×10^{-4}
Validation performance	2.46×10^{-4}
Test performance	3.92×10^{-4}
Gradient	4.23×10^{-7}
μ	1×10^{-6}
Validation Checks	6

Q_{max} (see Eq. 6) to calculate SOH. The ANN has an input layer, a hidden layer, and an output layer. Input layer has 3 neurons, hidden layer has 4 neurons (determined by trial and error), and output layer has only one neuron (SOH). The input data comprises of time (months), Storage temperature, and storage condition (fully-discharged or fully-charged). Similar to SOC, the input values of ANN are normalized between 0 and 1 by dividing the input value into absolute maximum input vector. The ANN output (CC-CV capacity) was also normalized by nominal capacity to represent SOH. Since CC-CV discharge capacities were measured at the end of CC-CV discharge, it consists of only 44 data points for various conditions. To decrease the error related to low data points, 2nd battery dataset which was originally used to determine the variability of cell capacity was also included in the training datasets (overall 88 data points). The ANN training results are given in Table IV. The MSE of 2.85×10^{-4} is achieved over test dataset equals to RMSE of 1.67%.

It takes 20 iterations to train ANN where the maximum 6 consecutive validation check condition was satisfied. The MSE variation for train, validation, and test datasets for SOH data is shown in Fig. 12a. Fig. 12b represents the error histogram for different datasets. Fig. 12b demonstrates that errors are distributed close to zero with the range below 0.04. This demonstrates the ANN capability to estimate SOH with high accuracy. Fig. 13 compares the SOH obtained from experiment with the one predicted by ANN. The results show that the ANN can successfully predict the battery SOH of calendared-age pouch cells.

Conclusions

In this study, the SOC and SOH of a calendar-aged commercial pouch cell consisting of NMC-LMO blended cathode and graphite anode have been estimated using ML approach. The calendar life of the cells has been evaluated at four different temperature and storage conditions. The ANNs used in this paper could map the measured battery data like voltage, current, aging time (months), storage temperature, and storage conditions, to the current SOC and SOH. In order to include LIB hysteresis effect during cycling, two separate ANNs were trained for SOC estimation during charge and discharge. The ANN achieved the RMSE of 1.17% over discharge and 1.81% over charge datasets. The SOH is estimated based

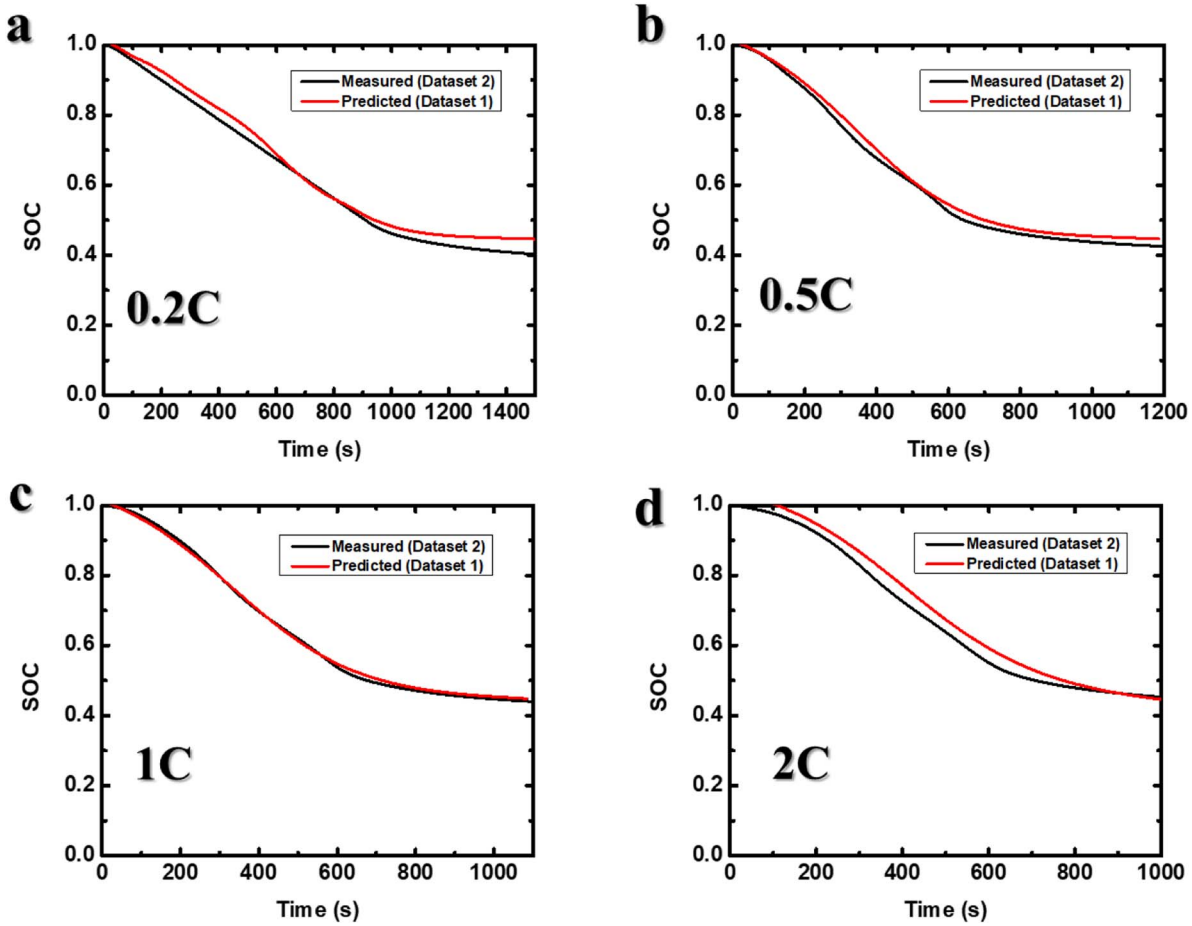

Figure 11. SOC after 8 months of aging (stored at 60°C- fully-charged) during discharge at various rates a) 0.2C b) 0.5C c) 1C d) 2C, measured based on dataset 2 (black), model prediction using dataset 1 (red).

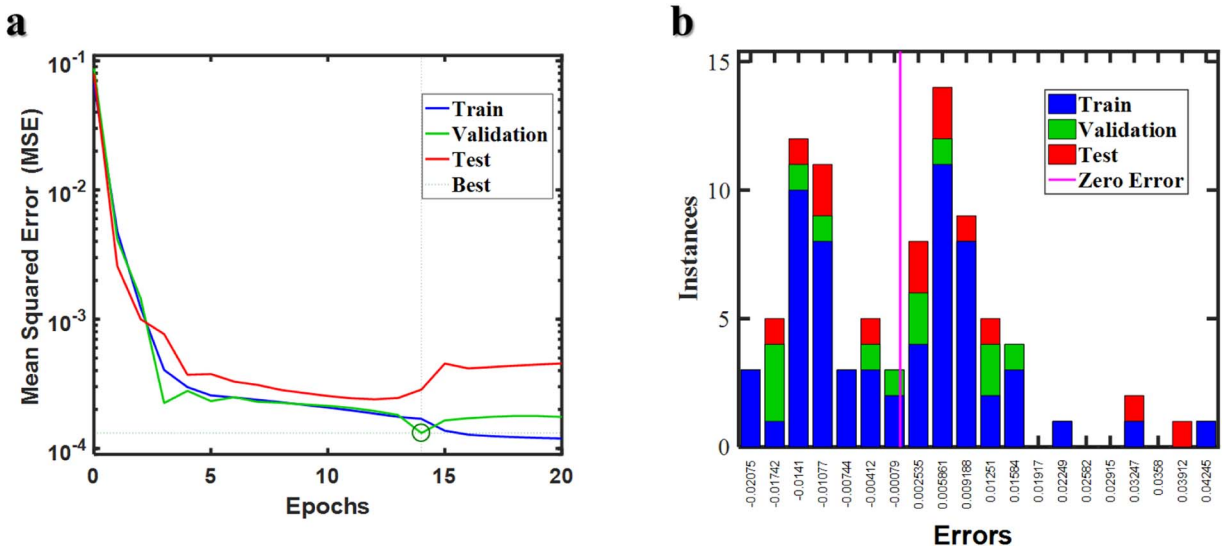

Figure 12. a) MSE for training, validation, and test datasets at different epochs for SOH, b) Error histogram which is the difference between target and ANN output.

on CC-CV discharge capacities at the end of C/5 discharge. The ANN achieve a RMSE of 1.67% over SOH test dataset, confirming the ability of the network to capture input-output dependency. It should be noted that the results and observation in this study are based on LIB pouch cells with NMC-LMO and graphite electrodes. Whereas different batteries with various electrode, electrolyte, components age differently, the proposed approach can be easily applied to other types of batteries. The current study improves the state-of-the-art of the SOC estimates to consider the batteries calendar aging.

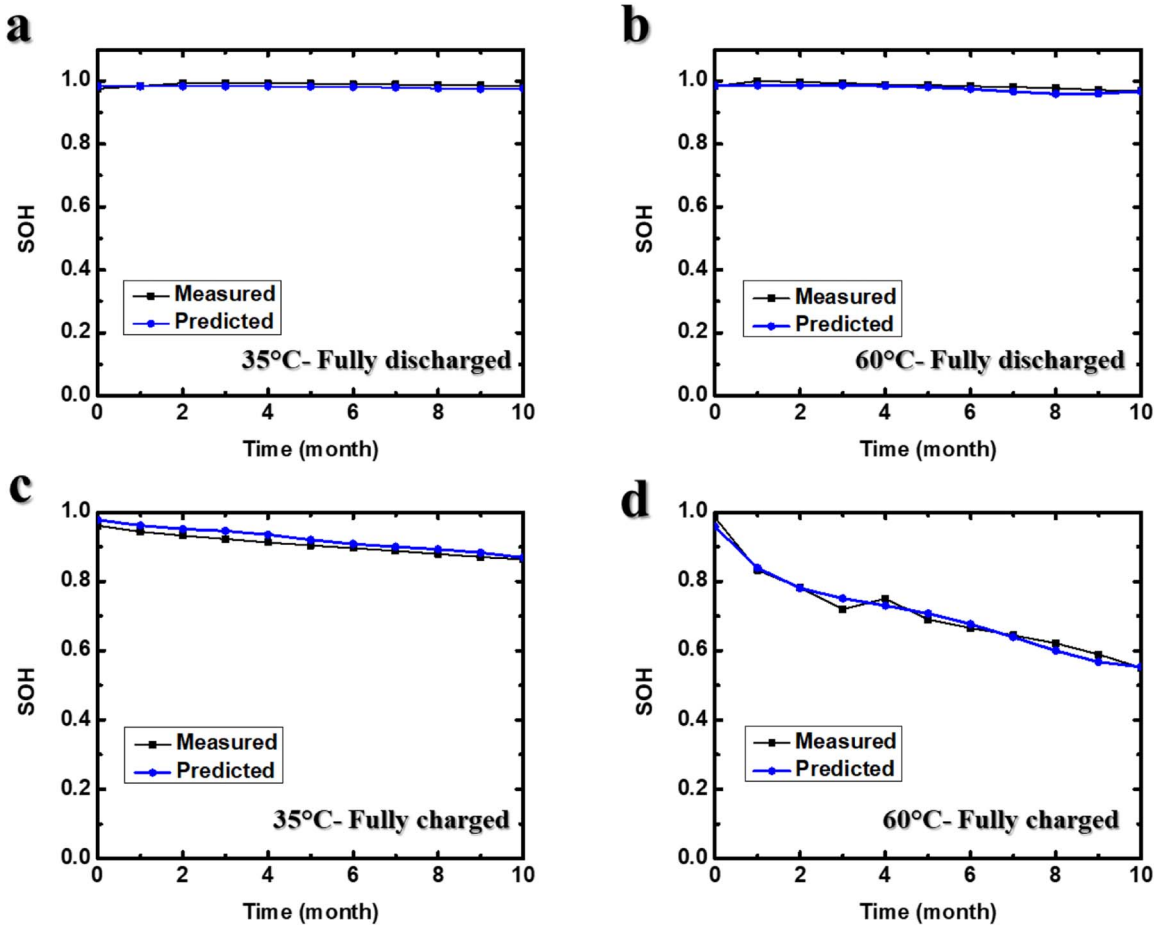

Figure 13. SOH estimation of calendar-aged pouch cells at various degradation conditions, measured (black) and ANN prediction (blue).

Acknowledgments

A.G.K. thanks Sam Ly for the insightful discussions. This research was supported by the Natural Sciences and Engineering Research Council of Canada (NSERC) through grants to Z.C. and the University of Waterloo.

List of Symbols

ANN	artificial neural network
b_j	bias of the hidden layer neuron j
h_j	activation function
i_j	total input of hidden layer
k	bias of the output layer neuron o
m	number of hidden layer neuron
p	number of neurons in the last hidden layer
MLP	multi-layer perceptron
MSE	Mean-Square-Error
n	number of observations
net o	total input of output layer (neuron o)
Q(t)	current capacity
Q_n	nominal capacity of fresh cell
Q_{max}	maximum releasable capacity fresh or aged cell
RMSE	Root-Mean-Square-Error
SOC	state of charge
SOH	state of health
t	time (s)
T	temperature (K)
x_i	input to the hidden layer neuron i and hidden layer neuron j
w_i	weight between the hidden layer neuron i and output layer neuron
w_{ij}	weight from hidden layer neuron i to hidden layer neuron j
y_i	measured value
$\widehat{y_i}$	predicted value

Greek

μ	parameter of Levenberg-Marquardt algorithm

ORCID

Ali Ghorbani Kashkooli https://orcid.org/0000-0002-0638-7133
Zhongwei Chen https://orcid.org/0000-0003-3463-5509

References

1. A. G. Kashkooli et al., *J. Appl. Electrochem.*, **47**, 281 (2017).
2. E. Foreman et al., *Adv. Sustain. Syst.*, **1700061**, 1700061 (2017).
3. A. G. Kashkooli et al., *J. Electrochem. Soc.*, **164**, A2861 (2017).
4. P. Röder et al., *J. Power Sources*, **268**, 315 (2014).
5. P. Keil et al., *J. Electrochem. Soc.*, **163**, A1872 (2016).
6. B. Stiaszny et al., *J. Power Sources*, **258**, 61 (2014).
7. K. Takahashi et al., *J. Electrochem. Soc.*, **163**, A385 (2016).
8. A. M. Grillet et al., *J. Electrochem. Soc.*, **163**, A1859 (2016).
9. A. Ghorbani Kashkooli et al., *Electrochim. Acta*, **247**, 1103 (2017).
10. B. Bitzer and A. Gruhle, *J. Power Sources*, **262**, 297 (2014).
11. C. Uhlmann, J. Illig, M. Ender, R. Schuster, and E. Ivers-Tiffée, *J. Power Sources*, **279**, 428 (2015).
12. N. Legrand, B. Knosp, P. Desprez, F. Lapicque, and S. Raël, *J. Power Sources*, **245**, 208 (2014).
13. S. P. Kim, A. C. T. V. Duin, and V. B. Shenoy, *J. Power Sources*, **196**, 8590 (2011).
14. N. Dupré et al., *J. Power Sources*, **196**, 4791 (2011).
15. M. Broussely et al., *J. Power Sources*, **146**, 90 (2005).
16. I. Buchberger et al., *J. Electrochem. Soc.*, **162**, A2737 (2015).
17. M. Wohlfahrt-Mehrens, C. Vogler, and J. Garche, *J. Power Sources*, **127**, 58 (2004).
18. J. Vetter et al., *J. Power Sources*, **147**, 269 (2005).
19. J. Ye, A. Emadi, R. Gu, P. Malysz, and H. Yang, *IET Electr. Syst. Transp.*, **6**, 136 (2016).
20. E. Chemali, M. Preindl, P. Malysz, and A. Emadi, *IEEE J. Emerg. Sel. Top. Power Electron.*, **4**, 1117 (2016).
21. L. McCurlie, M. Preindl, and A. Emadi, *IEEE Trans. Ind. Electron.*, **64**, 1350 (2017).
22. R. Ahmed, M. El Sayed, I. Arasaratnam, Jimi Tjong, and S. Habibi, *IEEE J. Emerg. Sel. Top. Power Electron.*, **2**, 659 (2014).
23. R. Xiong, J. Cao, Q. Yu, H. He, and F. Sun, *IEEE Access*, **6**, 1832 (2018).
24. W.-Y. Chang, *ISRN Appl. Math.*, **2013**, 1 (2013).
25. E. Chemali, P. J. Kollmeyer, M. Preindl, R. Ahmed, and A. Emadi, *IEEE Trans. Ind. Electron.*, **65**, 6730 (2018).
26. X. Hu, F. Sun, and Y. Zou, *Energies*, **3**, 1586 (2010).
27. J. Li, J. Klee Barillas, C. Guenther, and M. A. Danzer, *J. Power Sources*, **230**, 244 (2013).
28. J. Xu et al., *IEEE Trans. Veh. Technol.*, **63**, 1614 (2014).
29. I. S. Kim, *IEEE Trans. Power Electron.*, **25**, 1013 (2010).
30. H. Hongwen, X. Rui, Z. Xiaowei, S. Fengchun, and F. JinXin, *Veh. Technol. IEEE Trans.*, **60**, 1461 (2011).
31. G. L. Plett, *J. Power Sources*, **134**, 277 (2004).
32. H. Dai, X. Wei, Z. Sun, J. Wang, and W. Gu, *Appl. Energy*, **95**, 227 (2012).
33. M. Mastali et al., *J. Power Sources*, **239**, 294 (2013).
34. M. A. S. Y. Zhang, K. K. Shin, and X. Tang, US20120072144 (2012).
35. A. K. A. A. Syed, B. J. Koch, and S. Schaefer, US20120109556 (2012).
36. C. B. C. Anil Paryani, Scott Ira Kohn, Brian Boggs, and Andrew David Baglino, US8004243 B2 (2011).
37. M. J. G. J. Lin, X. Tang, B. J. Koch, and D. R. Frisch, US7768233 (2010).
38. Y. Li, US8706333 (2014).
39. G. L. Plett, US8103485 B2 (2012).
40. Y. Lecun, Y. Bengio, and G. Hinton, *Nature*, **521**, 436 (2015).
41. N. Dawson-Elli, S. B. Lee, M. Pathak, K. Mitra, and V. R. Subramanian, *J. Electrochem. Soc.*, **165**, A1 (2018).
42. I. Cho, EP1702219B1 (2012).
43. D. Y. J. I. Cho and D. Y. Kim, US8626679 (2014).
44. W. Y. Chang, *Int. J. Electr. Power Energy Syst.*, **53**, 603 (2013).
45. E. Chemali, P. J. Kollmeyer, M. Preindl, and A. Emadi, *J. Power Sources*, **400**, 242 (2018).
46. P. Singh, R. Vinjamuri, X. Wang, and D. Reisner, *J. Power Sources*, **162**, 829 (2006).
47. T. Zahid, K. Xu, W. Li, C. Li, and H. Li, *Energy*, **162**, 871 (2018).
48. J. N. Hu et al., *J. Power Sources*, **269**, 682 (2014).
49. V. Klass, M. Behm, and G. Lindbergh, *J. Power Sources*, **270**, 262 (2014).
50. M. Charkhgard and M. Farrokhi, *IEEE Trans. Ind. Electron.*, **57**, 4178 (2010).
51. J. Meng, G. Luo, and F. Gao, *IEEE Trans. Power Electron.*, **31**, 2226 (2016).
52. G. Davies et al., *J. Electrochem. Soc.*, **164**, A2746 (2017).
53. R. Spotnitz, *J. Power Sources*, **113**, 72 (2003).
54. M. Berecibar et al., *J. Power Sources*, **320**, 239 (2016).
55. C. Hu, B. D. Youn, and J. Chung, *Appl. Energy*, **92**, 694 (2012).
56. Z. Mao, M. Farkhondeh, M. Pritzker, M. Fowler, and Z. Chen, *J. Electrochem. Soc.*, **164**, A3469 (2017).
57. T. M. Mitchell, *Commun. ACM*, **42**, 30 (1999).
58. C. M. Bishop, *Neural networks for pattern recognition.* Oxford University Press, (1995).
59. J. J. Moré, "The Levenberg-Marquardt algorithm: Implementation and theory." In: Watson G.A. (eds) *Numerical Analysis. Lecture Notes in Mathematics*, vol 630. Springer, Berlin, Heidelberg (1978).
60. Z. Mao, M. Farkhondeh, M. Pritzker, M. Fowler, and Z. Chen, *J. Electrochem. Soc.*, **164**, A39 (2017).
61. M. A. Roscher and D. U. Sauer, *J. Power Sources*, **196**, 331 (2011).